Eur Biophys J (1989) 16:327–339

European Biophysics Journal

A molecular dynamics study of the *C*-terminal fragment of the L7/L12 ribosomal protein

II. Effects of intermolecular interactions on structure and dynamics

J. Åqvist, M. Leijonmarck, and O. Tapia

Department of Molecular Biology, Swedish University of Agricultural Sciences, and Uppsala University, Uppsala Biomedical Centre, Box 590, S-75124 Uppsala, Sweden

Received September 7, 1987/Accepted in revised form September 21, 1988

Abstract. The crystallographic dimer of the *C*-terminal fragment (CTF) of the L7/L12 ribosomal protein has been subjected to molecular dynamics (MD) simulations. A 90 picosecond (ps) trajectory for the protein dimer, 19 water molecules and two counter ions has been calculated at constant temperature. Effects of intermolecular interactions on the structure and dynamics have been studied. The exact crystallographic symmetry is lost and the atomic fluctuations differ from one monomer to the other. The average MD structure is more stable than the X-ray one, as judged by accessible surface area and energy calculations. Crystal (non-dimeric) interactions have been simulated in another 40 ps trajectory by using harmonic restraints to represent intermolecular hydrogen bonds. The conformational changes with respect ot the X-ray structure are then virtually suppressed.

The unrestrained dimer trajectory has been scanned for cooperative motions involving secondary structure elements. The intrinsic collective motions of the monomer are transmitted via intermolecular contacts to the dimer structure.

The existence of a stable dimeric form of CTF, resembling the crystallographic one, has been documented. At the cost of fairly small energy expenditure the dimer has considerable conformational flexibility. This flexibility may endow the dimer with some functional potential as an energy transducer.

Key words: Molecular dynamics, ribosomal protein, L7/L12-CTF, energy transducer, protein dimer interactions, conformational flexibility, structural fluctuation

1. Introduction

There is considerable indirect evidence that protein flexibility and fluctuations are essential for their biological function. Although structural fluctuations can be measured experimentally, the fundamental connection to functional properties is still far from being thoroughly established. Molecular dynamics (MD) studies of proteins may provide invaluable information in this respect. The function of many proteins is related to the formation of molecular aggregates, e.g. dimers, trimers, tetramers etc. Knowledge concerning the changes in the dynamic properties of a monomeric structure upon incorporation into a larger oligomeric assembly may be of particular relevance for understanding various processes in molecular biology. MD calculations may help to elucidate some aspects of this problem, provided that reliable experimental structural data of the protein complexes are available. The dimeric form on the *C*-terminal fragment of the L7/L12 ribosomal protein (CTF) is an important case since it might have a functional role on the ribosome (Leijonmarck and Liljas 1987). The dynamics of this species may be the basis of functionally important motions.

The 150 ps MD trajectory of the CTF monomer, reported by Åqvist et al. (1985), showed several interesting features related to the motion of secondary structural elements. The most striking of these was a librational motion of the αB helix with a characteristic frequency of $\nu = 5\ \mathrm{cm}^{-1}$. Although the overall agreement with respect to the X-ray structure was found to be better than most other comparable MD simulations, some local discrepancies were identified and could also be rationalised (Åqvist et al. 1985). In the present study the model has been extended to include the CTF dimer, two counter ions and structurally bound water. We are thus addressing the question of what are the effects of increasing the complexity of the model, both with respect to structure and dynamics.

L7/L12 ribosomal protein is essential for efficient polypeptide synthesis in bacteria (Möller 1974; Pettersson and Kurland 1980). The *C*-terminal region appears to be the functional domain since it is essential for inducing the GTPase activity in elongation factors

like EF-Tu and EF-G (Möller et al. 1983). Two dimers of L7/L12 are bound to the 50S ribosomal subunit and have a fairly large independent mobility (Gudkov et al. 1982; Cowgill et al. 1984). The flexibility of L7/L12 is abolished by the binding of an EF-G · GDPCP complex to the ribosome (Gudkov and Gongadze 1984). It has been suggested by Möller et al. (1983) that a conformational change of L7/L12 may be important for the functioning of this protein during the translation process. Liljas and Leijonmarck (1987) have suggested that the crystallographic dimer may in fact be the active one found on the ribosome. The MD study of the crystallographic dimer may in this respect, provide significant information.

Deviations in the previous monomer simulation were mainly attributed to two different sources: (1) the potential function was inadequate with respect to the cis-trans representation of non-bonded 1–4 neighbour interactions. (2) The monomer was missing all intermolecular contacts present in the crystal. In this work the potential function has been modified to allow a correct account of the non-bonded 1–4 interactions. The dimer represents a minimum model for intermolecular contacts. In order to simulate the remaining crystal interactions an additional trajectory was calculated with crystal hydrogen bonds represented by harmonic restraints. A relatively short (40 ps) trajectory has also been generated for the isolated monomer, using the new potential, to gauge the effects of this.

2. Method and model

The MD calculations have been carried out with the GROMOS program package. The computational strategy employed here is the same as in previous MD studies by us (Åqvist et al. 1985, 1986). Net charges on fully charged side chains have been screened down to zero, retaining only partial charges. Bond length constraints were applied using the SHAKE algorithm (van Gunsteren and Berendsen 1977). The system was weakly coupled to a thermal bath (Berendsen et al. 1984) of temperature $T_0 = 277$ K. The potential energy function differs from that used by Åqvist et al. (1985) in one respect. The extended atom non-bonded Lennard-Jones parameters for 1–4 neighbours have been changed to allow for the presence of *cis*-conformations; the peptide unit now has a stable *cis*-conformer.

The starting model corresponds to the CTF dimer generated by the crystallographic two-fold symmetry (Leijonmarck and Liljas 1987), where two sulphate ions and 19 water molecules in close contact with the protein were also included (Fig. 1). The tetrahedral sulphate ion was electrically neutralised in order to be consistent with the protein representation. Multipolar interactions are, however, included since each oxygen has a partial charge of -0.36 charge units and the sulphur atom bears a charge of $+1.44$. The van der Waals' parameters for the oxygens correspond to those of the carboxyl oxygen type. The water is represented by the rigid SPC model (Berendsen et al. 1981). The total number of explicitly treated atoms in this system is 1259.

Compared to the first CTF monomer simulation (Åqvist et al. 1985), the present model is a step towards including surrounding medium effects on the dynamics of the CTF monomer. The dimer explicitly models protein-protein interactions. The inclusion of crystallographically observed water molecules cannot be expected, by itself, to represent "solvent effects". However, taken together with other features, this type of simulation differs from true in vacuo systems at least in two respects: (1) The zero net charge on acidic and basic side chains seems to be a reasonable first approximation of solvent screening effects, in particular since these residues are mostly situated on the surface of the molecule. Using fully charged side chains, without explicitly including solvent molecules in the simulation, usually results in a tendency for these to fold back onto the protein surface (see e.g. Ahlström et al. 1986). Comparisons show that eliminating the net charges prevents this from happening (Åqvist and Tapia, unpublished results), thus giving better agreement with X-ray data. (2) Coupling the system to a thermal bath is not only a way to control the temperature during the equilibration period, but it is also a mechanism for exchanging energy with the surroundings. The bath coupling used here (see Berendsen et al. 1984) corresponds to an exponential decay of global temperature fluctuations, with a characteristic time of τ, which is the coupling parameter. The kinetic energy of the solvent molecules was scaled separately with $\tau = 0.05$ ps, while $\tau = 0.1$ ps was used for the protein dimer.

To get an insight on the effects of intermolecular (non-dimeric) crystal interactions on the present system, another (40 ps) simulation where these are represented by harmonic restraints has been carried out (cf. Sect. 3.2). This was done in such a way that all direct, or water bridged, hydrogen bonds produced by the crystal environment (48 in total) are modelled by restraining the positions of the corresponding H-bonding partners of the dimer. The force constants for these restraints were chosen to correspond with equilibrium force constants for organic H-bonding systems ($k = 50$ kcal/mol · Å^2), and the harmonic terms were added to the potential energy function.

The initial configuration used to calculate the MD trajectory was obtained after energy minimisation of the crystal structure. After the potential energy had converged to within 0.001 kJ/mol, initial velocities from a Maxwellian distribution were assigned to all

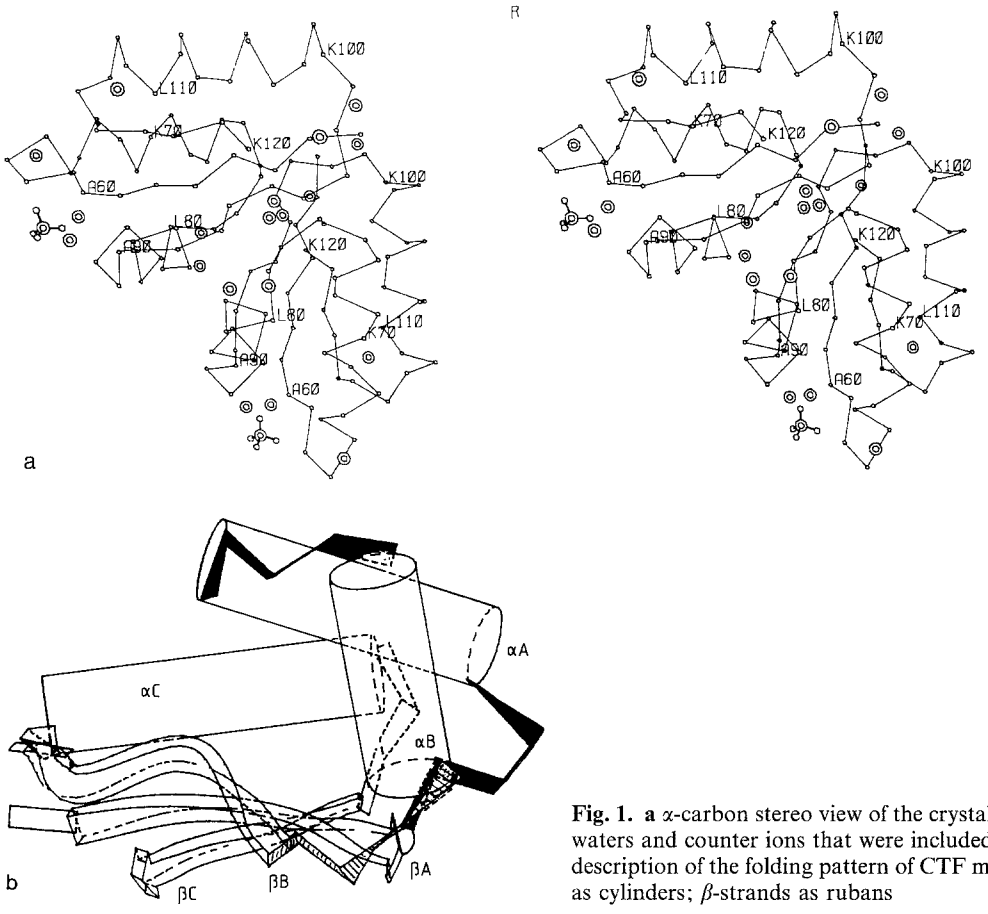

Fig. 1. **a** α-carbon stereo view of the crystallographic CTF dimer, with the waters and counter ions that were included in the simulations. **b** Pictorial description of the folding pattern of CTF monomer. α-Helices are depicted as cylinders; β-strands as rubans

atoms. The (unrestrained) trajectory lasted for 90 ps of which the first 20 ps correspond to an equilibration period.

When discussing average structures in the following sections we will use the following nomenclature. The average structures from the 20–90 ps part of the (unrestrained) dimer trajectory are denoted $\langle D20-90\rangle_{m1}$, $\langle D20-90\rangle_{m2}$, $\langle D20-90\rangle_{m12}$ and $\langle D20-90\rangle_{d}$. They correspond to the first and second time averaged monomer structure, the average of these two, and the average dimer structure, respectively. The restrained trajectory averages are denoted $\langle R10-40\rangle_{m1}$, $\langle R10-40\rangle_{m2}$, $\langle R10-40\rangle_{m12}$ and $\langle R10-40\rangle_{d}$. The average structure from the previously reported monomer simulation (Åqvist et al. 1985) is termed $\langle A20-150\rangle_{m}$ and $\langle B20-40\rangle_{m}$ denotes the average from a 40 ps simulation of the isolated monomer using the revised non-bonded potential (Åqvist and Tapia, unpublished results).

3. Results and discussion

The MD trajectory generated from the crystallographic dimer represents an equilibrated system where the dimer is fluctuating around a well defined average structure. The initial exact two-fold symmetry is rapidly broken, due to the independent assignment of random starting velocities from the Maxwell-Boltzmann distribution. Each monomer evolves in slightly different regions of the configuration (phase) space. The differences can be appreciated from Table 1, where the root mean square (rms) C_α coordinate deviations between the various average MD structures and the X-ray structure are reported. For symmetry reasons, the rms values for the two monomers would of course be interchanged if the initial velocities had been permuted and subjected to the symmetry operation.

When discussing results concerning the CTF monomer the $\langle D20-90\rangle_{m12}$ structure, i.e. where the average has been taken both over time and the two monomers, is used for comparison with the X-ray structure. Note that the rms deviations in Table 1 have been calculated after least squares fitting to all C_α's; this is the common procedure, but it can result in a distorted picture of the actual displacements, as we shall see below.

3.1 Average monomer structure

(i) Atomic positions. The rms coordinate deviations after least squares fitting to all the α-carbons, between

Table 1. Rms C_α coordinate deviations between various MD average monomer structures and the X-ray structure. The values are obtained after pairwise least squares fitting to all C_α's

	X-ray	$\langle A20-150\rangle_m$	$\langle B20-40\rangle_m$	$\langle D20-90\rangle_{m12}$	$\langle D20-90\rangle_{m1}$	$\langle D20-90\rangle_{m2}$	$\langle R10-40\rangle_{m12}$	$\langle R10-40\rangle_{m1}$	$\langle R10-40\rangle_{m2}$
X-ray	–	1.06	1.15	1.42	1.34	1.58	0.80	0.59	1.06
$\langle A20-150\rangle_m$		–	0.97	1.18	1.14	1.34	1.02	0.92	1.19
$\langle B20-40\rangle_m$			–	0.96	0.92	1.12	0.96	0.96	1.06
$\langle D20-90\rangle_{m12}$				–	0.37	0.37	1.24	1.22	1.33
$\langle D20-90\rangle_{m1}$					–	0.74	1.13	1.13	1.22
$\langle D20-90\rangle_{m2}$						–	1.44	1.40	1.53
$\langle R10-40\rangle_{m12}$							–	0.32	0.32
$\langle R20-40\rangle_{m1}$								–	0.63
$\langle R20-40\rangle_{m2}$									–

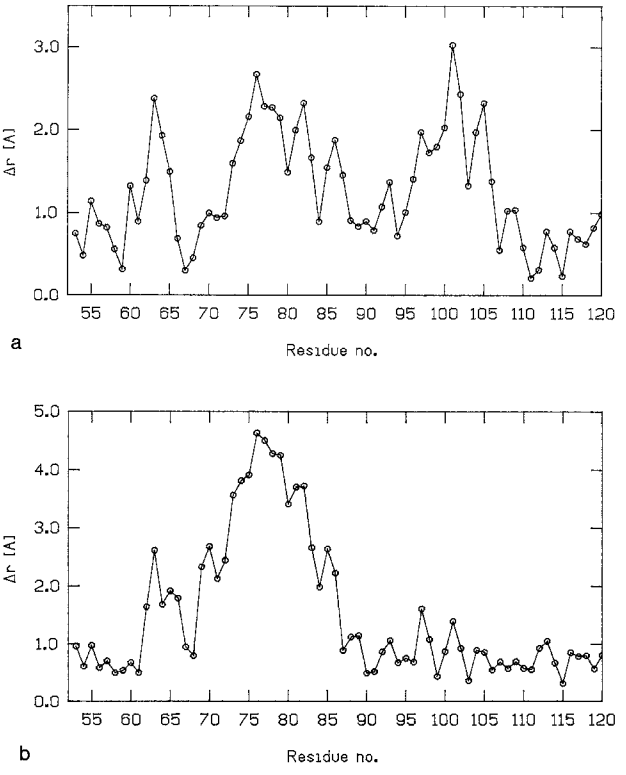

Fig. 2a and b. C_α coordinate deviations between $\langle D20-90\rangle_{m12}$ and the X-ray structure after least squares fitting to (**a**) all C_α's and (**b**) excluding residues 62–89

$\langle D20-90\rangle_{m12}$ and the X-ray structure are 1.42 Å and 1.92 Å for C_α's and all atoms, respectively. These figures are slightly larger than for the earlier monomer simulation ($\langle A20-150\rangle_m$) (cf. Table 1). The effect of the new potential is apparently not responsible for the increased deviation, as the rms value for C_α's of $\langle B20-40\rangle_m$ with respect to the X-ray structure is smaller than for $\langle D20-90\rangle_{m12}$, $\langle D20-90\rangle_{m1}$ and $\langle D20-90\rangle_{m2}$. Moreover, the C_α deviation between $\langle A20-150\rangle_m$ and $\langle B20-40\rangle_m$ is quite small (0.97 Å). Analysis shows that the new potential prevents the cis-trans isomerisation of Pro91, found in $\langle A20-150\rangle_m$. The differences between $\langle D20-90\rangle_{m12}$ and the crystallographic monomer have to be interpreted in terms of internal structural changes due to subunit interactions and to lack of other intermolecular (crystal) contacts.

In Fig. 2a the differences for C_α's are shown as a function of the residue number. A comparison of this figure to Fig. 3 of Åqvist et al. (1985) shows interesting similarities as well as differences. The former are important: the regions corresponding to β-structure have the smallest deviations with respect to the crystal structure, except perhaps for a couple of residues in βB. Therefore ist can be concluded that the β-pleated sheet, in particular its core, is a robust structural feature.

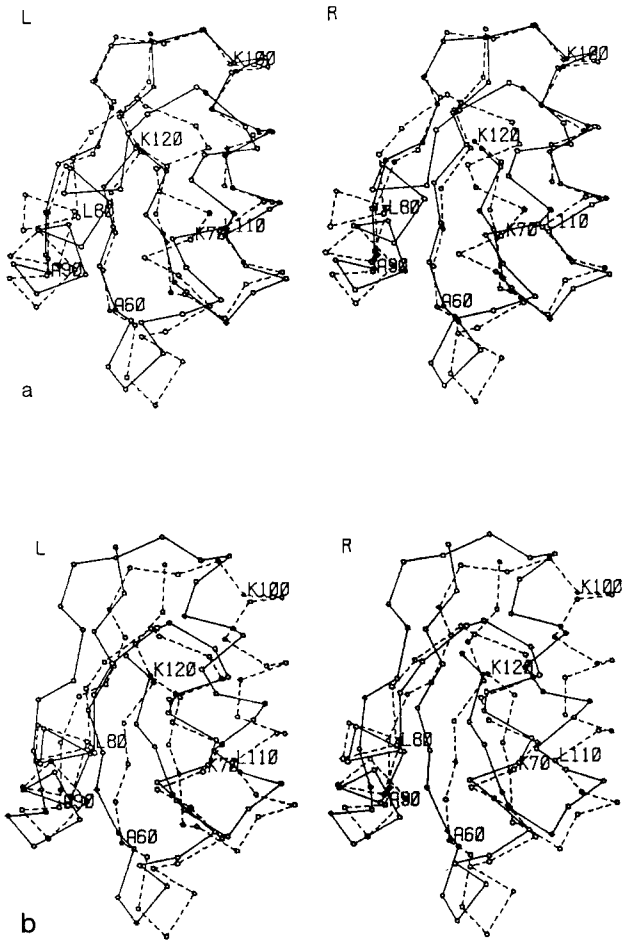

Fig. 3. Superposition of the X-ray structure (*dashed*) and $\langle D20-90\rangle_{m12}$. **a** Least squares fit to all C_α's except 62–89, **b** least squares fit to residues 62–89 only

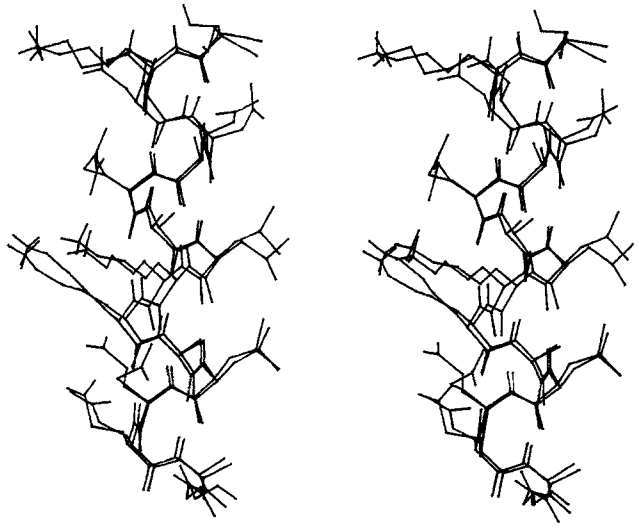

Fig. 4. Stereo view of the αC-helix from $\langle D20-90\rangle_{m1}$ superimposed on the X-ray structure. External side chains are on the left side of the helix, and internal ones on the right

The rms C_α coordinate deviation with respect to X-ray after least squares fitting to the β-structure only (19 atoms according to the definitions by Kabsch and Sander 1983) is just 0.67 Å. Inspection of the obtained fit (not shown) shows that the positions for αC are also in good agreement, while large deviations are found for residues 62–89. By including all C_α's except 62–89, the rms value becomes 0.79 Å (40 atoms). The corresponding superimposed structures are depicted in Fig. 3 a; in Fig. 2 b the differences for C_α's as a function of the residue number, for this fit, are given.

The rms deviations of C_α's seen from the robust part of the monomer suggest a rigid body displacement of the whole region 62–89. This is confirmed by fitting the $\langle D20-90\rangle_{m12}$ and X-ray structures to the C_α's of this region, which yields a deviation of 0.83 Å. Figure 3 b shows the corresponding superposition of the monomers.

Perusal of Fig. 2 a and b show that they have similar deviation patterns, but with very different absolute values. A comparison of Figs. 2 b and 3 of Åqvist et al. (1985) also reveals some similar features. Deviations above 1 Å are found for residues in the regions 62–66 and 75–89. In the $\langle D20-90\rangle_{m12}$ structure the differences for the stretch 69–86 are considerably larger, but as illustrated in Fig. 3 b they reflect a rigid body movement of the whole area.

It is interesting to note that, independently of the way the fitting is carried out, the reverse turn between βA and αA is badly reproduced. This is where the counterions are positioned in the crystal structure. Although these have been included in the present simulation, it is evident that they are not sufficient to maintain the X-ray conformation of the turn. This is not surprising since numerous intermolecular (non-dimeric) crystal contacts are present in this region (Leijonmarck and Liljas 1987) and probably play a more dominant role in fixing the conformation.

In spite of the rigid body displacement observed for the αA-αB unit, the local backbone structure is not sizably changed. It should also be mentioned that the atomic positions of side chains agree reasonably well with the X-ray structure. Since CTF contains quite a few long surface side chains (19 out of 68 are Arg, Lys, or Glu), one would perhaps expect larger deviations. It seems, however, that the screening of charges is a successful approach in this context. As an example, the agreement with respect to the X-ray structure for one of the αC helices is shown in Fig. 4. It is clear that the deviations for the exterior side chains, in this case, are not much larger than for the interior ones.

(ii) Backbone dihedral angles. It was recognised in the previous CTF simulation (Åqvist et al. 1985) that the non-bonded repulsion for the united atoms (CH, CH_2, CH_3) separated by three bonds was too large to allow

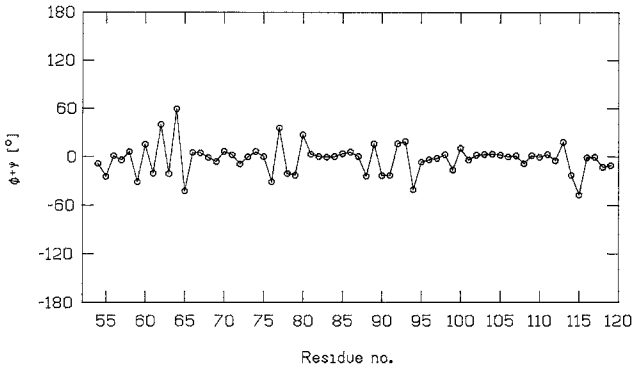

Fig. 5. Differences between $\langle D20\text{–}90\rangle_{m12}$ and the X-ray structure for $\phi + \psi$ as a function of residue number

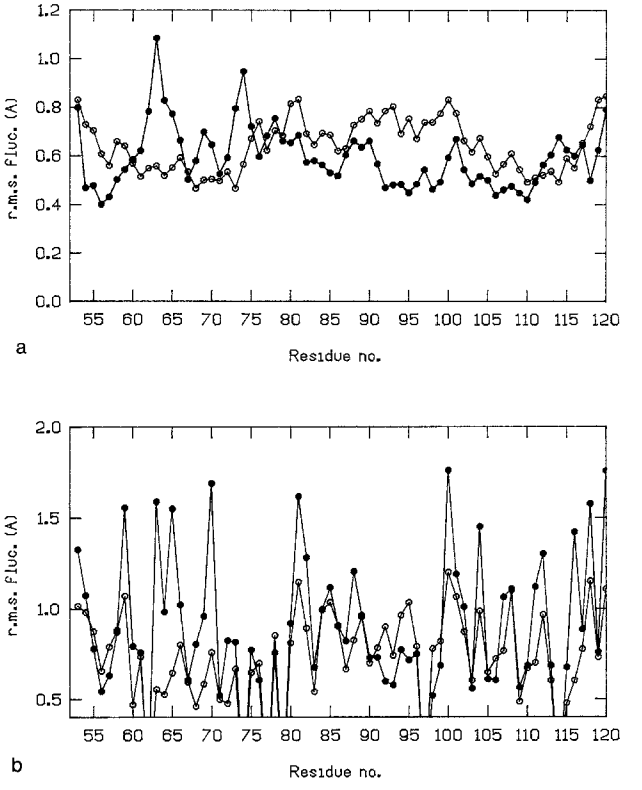

Fig. 6a and b. Rms positional fluctuations per residue, averaged over (**a**) backbone atoms and (**b**) side chain atoms. *Filled circles* denote MD fluctuations and *open circles* are those calculated from the crystallographic *B*-factors

proline residues to be in the *cis*-conformation. The average structure obtained with the revised potential shows that this undesired effect has now been removed; the peptide ω angle between Ala90 and Pro91 is now correct. Figure 5 shows the sum of the ϕ and ψ angles, for each residue. This function approximately represents the twist of a residue (Tainer et al. 1982). It can be seen that the agreement for the backbone angles has indeed improved with the new potential energy function, as compared to Fig. 6a of Åqvist et al. (1985). The rms deviation for the (ϕ, ψ) angles, with respect to the X-ray structure, is (13.0°, 16.8°); for ω-angles it is 3.4°. Hence, the conformation of the peptide backbone is well reproduced by the simulation. The regions where the largest differences are found for $\phi + \psi$ correspond to the loops βA-αA, αA-αB, αB-βB and αC-βC, while the ordered secondary structure presents only small deviations.

(iii) Hydrogen bonds. The present potential energy function contains no special hydrogen bonding term. Atoms which can form H-bonds may, due to electrostatic attraction between partial charges, spend enough time in the vicinity of each other during the trajectory to show up within H-bonding distances in the average structure. However, an average MD structure is usually one of very high potential energy, since bond lengths and angles are not neccessarily regular after the averaging procedure. For instance, an NH_3 group where the hydrogens rotate freely may in the average structure have all three hydrogens on top of each other. In our case, hydrogen bonding can only be defined in terms of a distance and angle criterion. We use here the energy minimised average structure calculated for the entire dimer when comparing H-bonds. For a listing of H-bonds in the crystal structure of CTF, the reader is referred to Åqvist et al. (1985) and Leijonmarck and Liljas (1987).

In the present simulation all of the backbone H-bonds found in the X-ray structure also occur in at least one of the average monomer structures from the dimer. There are now also several H-bonds involving side chain atoms, which was not the case in the previous simulation. The energy minimised X-ray structure has five (out of seven) of these in common with at least one of the MD monomers. In total the X-ray dimer has 30 H-bonds involving the 19 water molecules included in the simulation. The corresponding figure for the MD dimer is 37. Each monomer in the crystal structure has 13 H-bonds between protein atoms and the waters included here. Nine of these are reproduced by at least one monomer in the simulation. The hydrogen bonding pattern is thus in good agreement with the X-ray structure, although there are differences between the two monomers of the dimer.

(iv) Atomic positional fluctuations. The atomic positional fluctuations that can be derived from crystallographic temperature factors provide one of the most important experimental comparisons for theoretical MD calculations. In general the fluctuations calculated from crystallographic *B*-factors do not seem to be accurate enough for a detailed quantitative comparison to MD fluctuations (Kuriyan et al. 1986). On the other hand, they do provide a good basis for a qualitative discussion of the flexibility pattern. The

absolute values of the MD atomic rms fluctuations will depend on the length of the calculated trajectory, at least up to some limit of the time span. When averaging over successively longer parts of a trajectory, the magnitude of the fluctuations will increase rapidly for, say, 1 to 10 ps averages and then tend to some limiting value.

Figure 6 shows the atomic positional rms fluctuations averaged over the two monomers, and averaged per residue, for (a) backbone and (b) side chain atoms. It can be seen (Fig. 6a) that although the average MD fluctuations for the backbone are somewhat lower than the X-ray ones, the mobility pattern agrees well. An improvement of the patterns can be appreciated with respect to the previous CTF simulation, in particular for the loop region 76–79, where the two monomers interact in the dimer. However, there are still two parts of the peptide chain that display large differences when compared to the X-ray structure, namely the turn involving residues 61–64 and the *C*-terminal of αA around Gly74. In fact, both of these regions participate in non-dimeric intermolecular contacts (Leijonmarck and Liljas 1987), and it is reasonable to attribute the differences to these interactions.

Also for the side chains, the inclusion of the dimer interactions gives somewhat better agreement with the crystallographic *B*-factors, as can be seen from Fig. 6b. The largest deviations occur around the turn 62–63, Lys70 and Glu116, where in all cases intermolecular H-bonds are present in the crystal structure.

The positional fluctuations for long side chains are somewhat larger than indicated by X-ray *B*-factors. These side chains are mostly situated on the surface of the molecule and can therefore be expected to be found interacting (colliding) with the surrounding medium; such collision effects are not fully included in the present calculations. For the C_α, C_β, C_γ and C_δ carbons the MD fluctuations are 0.58, 0.68, 0.84 and 1.19 Å, respectively, whereas the crystallographic values are 0.63, 0.69, 0.84 and 0.93 Å (Leijonmarck and Liljas, unpublished results). As has been shown by Kuriyan et al. (1986), the commonly used procedure for X-ray structure refinement tends to underestimate the fluctuations of long side chains. This may also be reflected by the values given above.

When comparing the mobility of the few solvent molecules included in the simulation, one should keep in mind that the X-ray *B*-factors represent the fluctuations of solvent sites and not of individual molecules. The average rms fluctuation for the MD water oxygens is 1.71 Å, while the crystallographic value is 0.99 Å. This shows that some waters are not very tightly bound to the protein during the simulation. However, if one only considers the (13 out of 19) waters with MD rms fluctuations below 1.5 Å the agreement with the crystallographic mobility is rather good. In the simulation these water oxygens have an average mobility of 1.07 Å, compared to 1.04 Å in the crystal. The average MD mobility of the counter ion sulphur atoms is 1.05 Å, while the X-ray value is 1.10 Å. The individual rms fluctuations of the sulphur atoms are 0.79 Å and 1.32 Å, which reflects the fact that the latter of these has moved several Ångströms, from its initial to a new position, where it is not as tightly bound.

3.2 Asymmetry between monomers

The two monomers do not present symmetric trajectories. This is probably due to the assignment of initial velocities, which is illustrated e.g. by the rms deviations with respect to the X-ray structure: 1.98 Å for all atoms of monomer 1 and 2.10 Å for monomer 2. On the other hand, the corresponding rms difference between the two average MD monomers is slightly smaller (1.50 Å), which shows that they still have very similar structures.

The two monomers also present differences in the backbone atomic mobilities. While the rms fluctuations for monomer 1 agree better with the X-ray ones in the region 61–75, monomer 2 shows a better agreement in the region 79–95. The rms fluctuations averaged over all backbone atoms are 0.64 Å, 0.51 Å and 0.67 Å for the X-ray, $\langle D20-90\rangle_{m1}$ and $\langle D20-90\rangle_{m2}$ structures, respectively. Since the crystallographic monomers were not refined independently it is, however, difficult to assess the significance of the differentiated mobilities.

In the analysis of the previous CTF monomer trajectory (Åqvist et al. 1985) time correlation functions for the stretching of secondary structural elements were calculated. The stretching was then modelled by a vector connecting atoms at the two ends of the secondary structure. It was found that the αB helix had a fairly correlated longitudinal motion. Figure 7a shows the spectral density for the longitudinal stretching of αB in the 150 ps monomer simulation, but with the stretching represented by the projection of the vector connecting $C_\alpha 80 - C_\alpha 87$ on the instantaneous helix axis (Åqvist 1986). Qualitatively, the picture is the same for αB when using this representation of the stretching as compared to the previous one (Åqvist et al. 1985). It is clearly dominated by a frequency around 5 cm^{-1}.

In Fig. 7b and c, the corresponding spectral functions are shown for the two αB helices in the dimer trajectory. It can be appreciated that αB in monomer 2 has a very similiar longitudinal spectrum to that found in the simulation of the isolated monomer. In contrast, the same helix in monomer 1 presents clear differences, with the spectral density shifted to higher

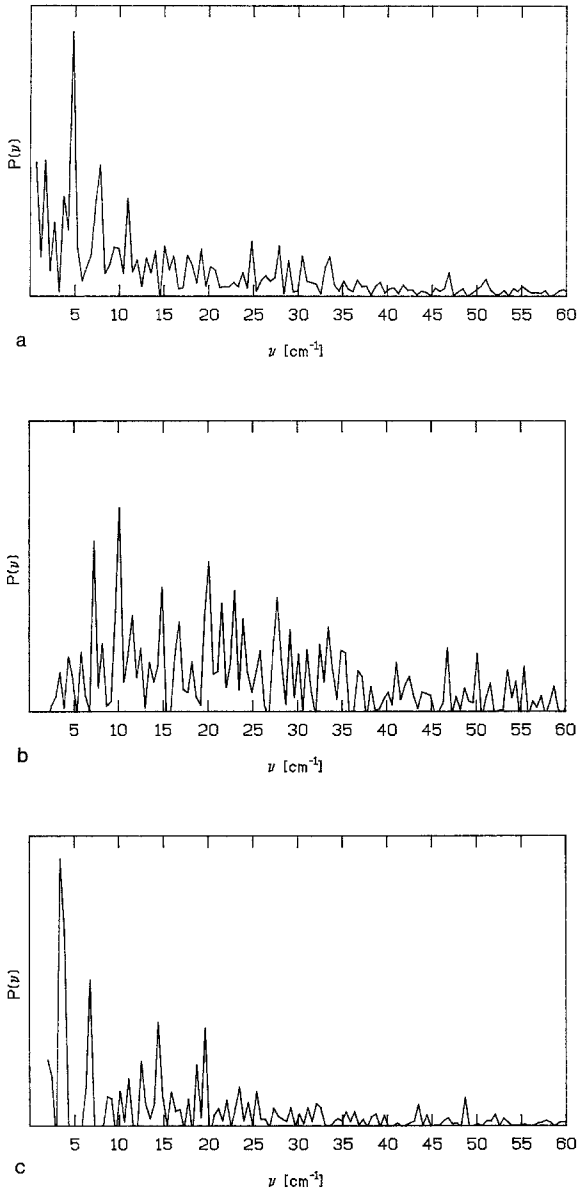

Fig. 7a–c. Spectral densities calculated for the longitudinal stretching of the αB-helix, (**a**) from the 20–150 ps monomer trajectory and from the 20–90 ps dimer trajectory, where (**b**) corresponds to monomer 1 and (**c**) to monomer 2

frequencies. This difference in the longitudinal motions of the αB helix in the two monomers can be related to slightly different structural properties of the relevant region.

The idea that low frequencies generally correspond to larger amplitudes is nicely illustrated by the present example. The rms amplitude of the αB_2 stretching (the subscript corresponds to the monomer number) is 0.43 Å, while it is 0.25 Å for αB_1. The smaller amplitude and higher frequencies for αB_1 indicate that there must be damping effects on the motions of this helix. In fact, the examination of hydrogen bonds in the region shows that these may be a source of the damping. In αB_2 the first H-bond Gly790-Ala83N, which is present in the X-ray structure as well as in αB_1, is switched to Gly790-Glu82N. Furthermore, αB_1 has side chain H-bonds between Lys84N_ζ-Glu880$_\varepsilon$ and Asp850$_{\delta 1}$-Ser890$_\gamma$ which are present 24% and 18% of the trajectory, respectively. There are also more H-bonds to solvent molecules in αB_1, in particular at its C-terminal. It thus seems reasonable to attribute the differences in the longitudinal vibrations of the helices to damping effects due to hydrogen bonds.

The αC helix in both monomers displays a power spectrum for the longitudinal mode that is similar to that found in the isolated monomer simulation (not shown).

3.3 Dimer structure

Leijonmarck and Liljas (1987) have proposed that the crystallographic dimer of CTF may represent naturally occurring contacts on the ribosome. It is therefore interesting not only to examine the effects of the dimeric interactions on the structure and dynamics of the simulated CTF monomer, but also to see whether this dimer model proves to be a stable species.

(i) Unrestrained simulation. The average dimer structure, superimposed on the X-ray structure is shown in Fig. 8. The coordinate deviations with respect to the X-ray dimer are 3.37 Å and 2.84 Å for all atoms and C_α's, respectively. These numbers are considerably larger than for the average monomer ($\langle D20-90\rangle_{m12}$). It may be appreciated from Fig. 8 that while the conformation of the dimer interface is fairly intact, a change in the relative orientation of the two monomers has occurred. This movement is most likely related to the rigid body displacements of the αA-αB motif, found in both average monomers. The energy minimised X-ray structure has a total of 14 H-bonds across the dimer interface, including those bridged by water molecules, involving atoms from ten residues on each monomer. In the average MD dimer, seven of these residues participate in interface H-bonds, although some of them have switched to another hydrogen bonding partner. The total number of H-bonds in the MD structure is nine, of which five are bridged by waters.

The change in orientation between the two monomers occurs during the equilibration period of trajectory. It appears mainly as a rotation of the monomers with respect to each other. The "axis" of this rotation is roughly perpendicular to the dimer interface, and is depicted in Fig. 8. Each monomer is rotated approximately 15° (positive rotation for one monomer and negative for the other) around this axis, thus giving a change of roughly 30° in the relative

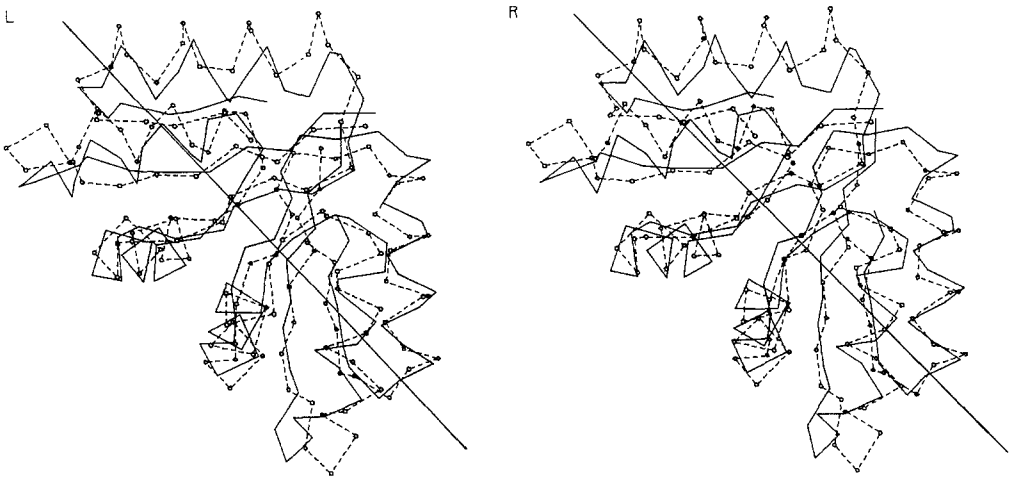

Fig. 8. Stereo view of the average MD dimer structure ($\langle D20-90\rangle_d$) superimposed on the X-ray dimer (*dashed*). An approximate rotation axis is also depicted

Table 2. Accessible surface areas (Å^2) for the X-ray and average MD structures. m_1+m_2-d is the area hidden in the dimer

	X-ray	MD ⟨20–90 ps⟩
Dimer (d)	6156	5525
Monomer ($m_1 : m_2$)	3309 : 3309	3065 : 3103
m_1+m_2-d	462	643

Table 3. Final energies (kcal/mol) after 800 steps of steepest descent minimisation using a cut-off radius of 8 Å for non-bonded interactions. (n) denotes screened net charges and (c) fully charged side chains. The superscripts *el*, *L-J* and *N B* represent electric, Lennard-Jones and total non-bonded energies, respectively. The subscripts 1–2, *p-p* and *p-w* denote interactions between different groups. 1–2: interactions between the monomers only, *p-p*: protein-protein (all atoms), *p-w*: protein-water

	el E 1–2	*L-J* E 1–2	*N B* E 1–2	*N B* E *p-p*	*N B* E *p-w*
X-ray (n)	−28.0	−59.9	−87.9	−1571	−223.9
$\langle 20-90\rangle_d$ (n)	−24.0	−83.0	−107.1	−1722	−279.5
X-ray (c)	−153.8	−43.6	−197.4	−4159	−413.3
$\langle 20-90\rangle_d$(c)	−346.3	−69.5	−415.8	−4181	−390.0

orientation, as compared to the X-ray structure. Furthermore, there is a tightening of the dimer interface in the MD simulation resulting in one water molecule in the interface moving out to form a hydrogen bond at the surface. Four other waters approach the interface region from the outside, thereby making closer contacts to the protein.

The tightening is also reflected by the fact that the molecular surface area that becomes hidden in the dimer is increased. In Table 2 the accessible surface areas, calculated with the MS program (Connolly 1983), corroborate this point quantitatively. We also note that the average MD dimer has a considerably smaller total accessible surface area than the crystallographic one.

A point of interest is the difference found in contact areas between the MD dimer and the X-ray structure. The former being larger than the latter. This result may elicit an intrinsic property of the dimer, namely, in vacuo such a structure tends to maximise the contact area, while in the crystal, intermolecular interactions (packing forces) might be sufficient to modify the relative orientation of the monomers and, consequently, decrease the contact area. If such an effect is true, it might well be of importance in connection with dimeric structural flexibility. Thus, to evaluate the order of magnitude involved in the intermolecular energies, some simple calculations were carried out. No attempt to introduce entropic terms is done at this level of analysis. Since the MD trajectory was calculated with all net charges on basic and acidic residues screened down to zero, this could affect energy differences. To test whether screening may bias the results or not, the X-ray and the average MD structure were energy minimised both with and without net charges on.

The results of the energy minimisations are summarised in Table 3. Each run of energy minimisation consisted of 800 steepest descent steps, using a cutoff radius of 8.0 Å for the non-bonded interactions. The results show that the electrostatic factor, in this case, is not likely to affect the conclusions derived from the MD simulation. Both sets of charges give lower total monomer-monomer interaction energy for the MD structure, the difference being 218 and 19 kcal/mol with and without charges, respectively. The energy difference corresponds to 5.1% of the total non-

bonded energy of the system with charges, and 1.2% of the uncharged system.

The differences in accessible surface area and "subunit" interaction energies thus indicate that the average MD structure is more favourable energetically, in view of the present potential energy function. The question of whether non-dimeric crystal contacts are enough to force the dimer into its X-ray conformation, thus preventing the observed orientational change, is therefore an interesting one.

(ii) Restrained simulation. The most rigorous way of assessing the role of intermolecular crystal interactions would be to include the full crystallographic unit cell in an MD simulation. Such a calculation would, however, be very time consuming since the unit cell contains eight CTF monomers and several thousand water molecules. As a preliminary attempt to investigate this issue, we have performed a 40 ps simulation of the CTF dimer, with the crystallographic H-bonds between non-dimeric neighbouring molecules mimicked by simple (weak) harmonic potentials. The value of the harmonic force constant was chosen as 50 kcal/(mol · Å^2), roughly in correspondence with the equilibrium force constant of a hydrogen bond. In this manner a total of 48 atoms in the CTF dimer were restrained, all of which participate in direct or water bridged intermolecular H-bonds.

Figure 9 shows the average restraint dimer structure, calculated from the 10–40 ps part of this trajectory. The rms coordinate deviations with respect to the X-ray structure are 1.16 Å (all atoms) and 0.80 Å (C_α's) for the average monomer, and 1.46 Å (all atoms) and 0.89 Å (C_α's) for the whole dimer (see also Table 1 for comparisons). As is evident from Fig. 9, the rotation of the monomers observed for the free dimer does not occur in this case.

It can be seen from Table 3 that the total protein non-bonded potential energy for the minimised $\langle D20-90\rangle_d$ structure is about 150 kcal/mol lower than for the X-ray structure (zero net charges). This difference is basically due to intra monomer stabilisation effects; the intermolecular interaction energy contributes about 20 kcal/mol to the stability of the MD dimer. The energy barrier between the two conformations is evidently smaller than the available kinetic energy, as the system drifts irreversibly to the average MD potential well. The average energy of the restraints in the restrained simulation is 37 kcal/mol, which shows that a barrier of, at most, this height is required to prevent the drifting. The energy per restraint atom is surprisingly small: 0.8 kcal/mol. Such a figure is in the range of what can be achieved with hydrogen bonds between uncharged groups (Fersht et al. 1985).

With charged side chains, the energy minimised structures derived from X-ray and $\langle D20-90\rangle_d$ show that the MD dimer is still the more stable. The total non-bonded protein energy difference is, however, smaller than with zero net charges: 22 kcal/mol. This quantity results as a compromise between favourable intermolecular interactions and less favourable intra monomer interactions. The important issue here is not the actual numbers, but the fact that the energy differences between the potential wells can be modulated by external sources acting on the state of charge of the acidic and basic side chains.

3.4 Collective motion

One of the features found in the previous trajectory of the CTF monomer (Åqvist et al. 1985) was a librational mode of the αB helix with respect to the rest of the

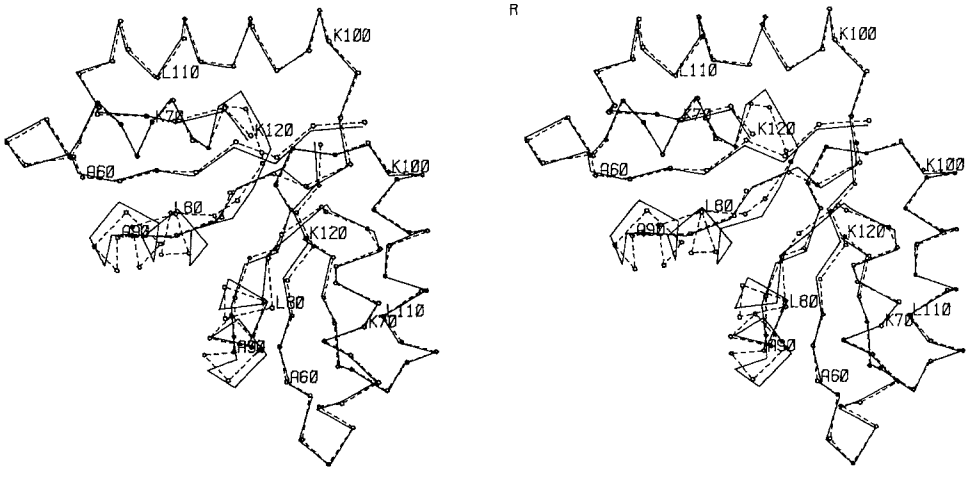

Fig. 9. View of the average MD restrained dimer structure ($\langle R10-40\rangle_d$) superimposed on the X-ray dimer (*dashed*)

molecule. The frequency of this highly collective motion was roughly 5 cm^{-1}. The analysis of the average monomer structure resulting from the 90 ps dimer simulation suggests a differentiation of two supersecondary structures: the right handed $\alpha\alpha$-corner (αA-short loop – αB) and the $\beta\alpha\beta$ unit plus the intercalated βA strand making the twisted β-sheet ($\beta\alpha\beta+\beta$). In fact, further analysis of the 20–150 ps monomer trajectory using the helix axes, instead of interatomic vectors, to characterise relative motions shows that αA is also affected by the libration of αB. Its relative motion with respect to αC is also dominated by frequencies around 5 cm^{-1}, although the spectrum is not as sharply peaked as for αB. The motion may thus be described as a libration involving the whole right handed $\alpha\alpha$-corner, hinged to the $\beta\alpha\beta+\beta$ domain. This motion can be affected by the dimer interactions, as the loop connecting αA to αB is partly involved in the intermolecular (dimer) contacts. This effect is reflected by the backbone rms fluctuations (cf. Fig. 6a), which show a clear damping in this region, when compared to the monomer results. It is therefore interesting to see how the dimer interactions, as reflected by the present trajectory, affect this and other dynamic properties in the monomer.

The present trajectory has been scanned for collective motions, involving secondary structure elements, by calculating axes representing α-helices and β-strands (see Åqvist et al. 1986). Power spectra and time correlation functions were calculated for scalar products between various pairs of secondary structure element axes.

Interestingly, the same frequency of 5 cm^{-1}, as found for the right handed $\alpha\alpha$-corner in the monomer, now appears as characteristic of the relative motion of the two monomers with respect to each other. Figure 10 shows two extreme positions of the relative orientation of the monomers. These orientations appear to be related mainly by a rotation around an axis through the dimer interface, and perpendicular to the plane of the drawing. The time correlation function for the scalar product between the axes of the two αC helices is shown in Fig. 11 a, and for the axes representing the two βA strands in Fig. 11 b. It can be seen from the correlation functions that the motion has a correlation time of 6.5–7.0 ps. The spectral density for the relative motion of the two αC helices is shown in Fig. 11 c. The same frequency peak at about 5 cm^{-1} also appears, for example, for the relative motion between the pair of βA : s and αB : s (not shown). For the pair of αB helices, the spectrum also contains additional higher frequency contributions. This may reflect the fact that the relative subunit motion gives the smallest amplitudes close to the "rotation axis". The angle between the two αC helices may be used to give an idea of the amplitude of the motion. The amplitude of the fluctuations in this angle varies from a few degrees up to a maximum of 10°.

4. General discussion

The crystallographic dimer of the *C*-terminal fragment of the L7/L12 ribosomal protein has been studied by molecular dynamics simulations. A 90 ps trajectory was computed for a system comprising the CTF dimer, some crystallographically observed waters and two counter ions. The MD simulation leads to an average dimer structure differing slightly form the crystallographic one. Crystal packing effects have been simulated in another trajectory (40 ps long) by using harmonic restraints to mimic intermolecular (non-dimeric) hydrogen bonds. As the model approaches the crystal situation, the trends in terms of deviations

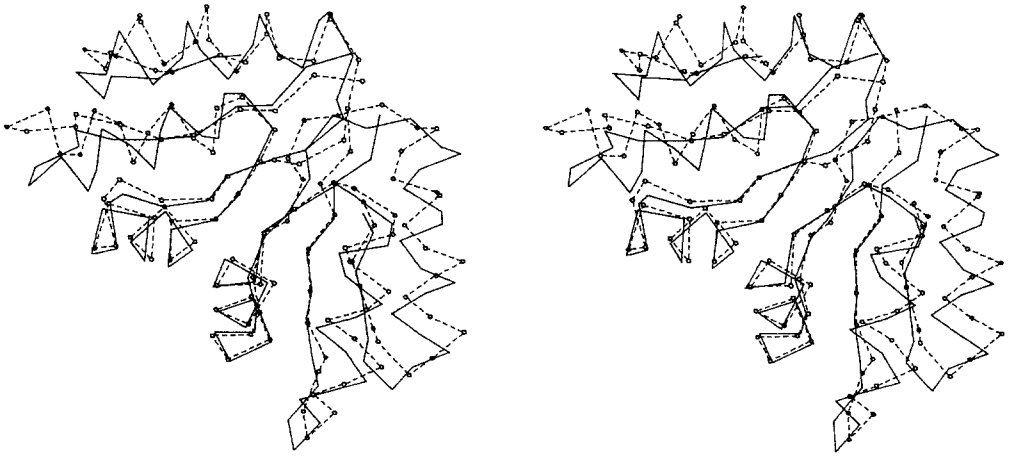

Fig. 10. Two extreme positions, adjacent in time, for the relative orientation between the monomers, reflecting the motion for which the 5 cm^{-1} frequency is observed

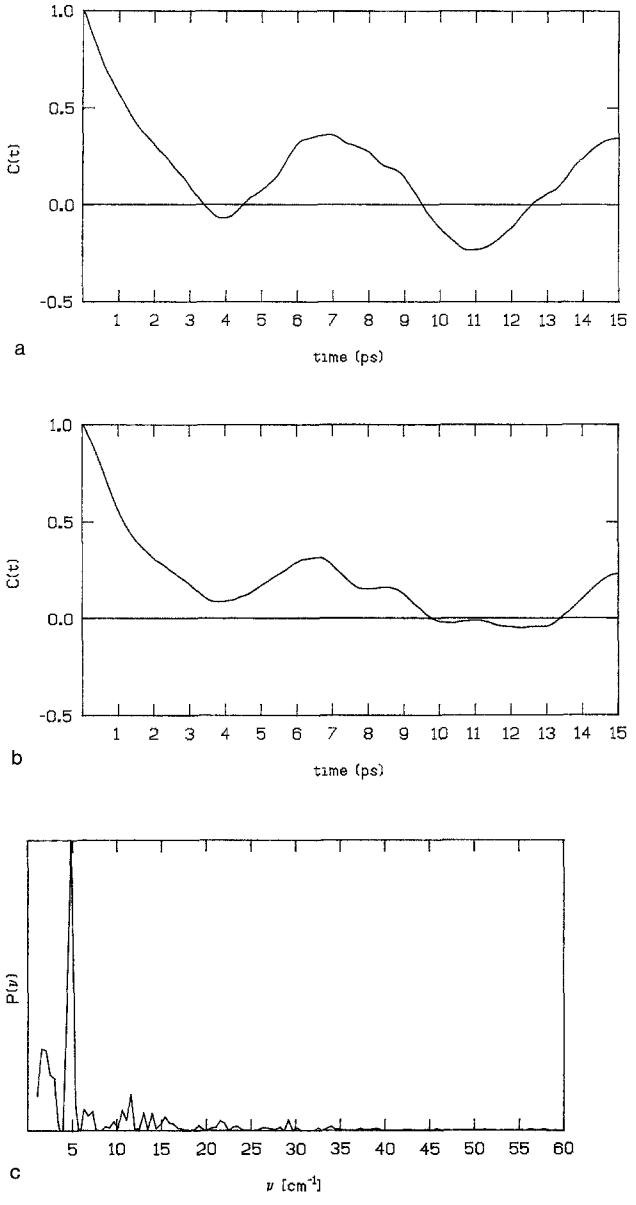

Fig. 11a–c. Time correlation functions for the scalar product between the axes characterising (**a**) the two αC-helices and (**b**) the two βA-strands, and (**c**) the spectral density for the relative motion of the αC-helices

in atomic positions and fluctuations indicate an improved agreement with experimental data. The existence of a stable dimeric form of CTF, resembling the crystallographic one, has been firmly documented in this study. For fairly low energy expenditure, the dimer has considerable conformational flexibility, which may provide functional potential.

From the trajectory of the unrestrained dimer, important aspects concerning the effects of subunit interactions on the monomer behaviour emerge. The characteristic frequency of the helix libration (5 cm^{-1}), observed for the free monomer, is retained, but mainly due to interactions involving the right handed $\alpha\alpha$-corner, the motion appears as a fluctuation in the relative orientation of the monomers.

Subunit interactions force a structural and dynamic differentiation in the monomers. The two supersecondary structural motifs of the monomer have been displaced in a rigid body manner with respect to each other. Interestingly, the average monomer structure is fairly similar to the instantaneous structure corresponding to one of the extreme positions for the αB helix in the previous monomer simulation (cf. Fig. 11 of Åqvist et al. 1985). This indicates that the αA-αB unit has been trapped in one of the extreme conformations observed in the monomer.

The αA-αB loop and the *N*-terminal of αB in one subunit makes contacts with the αB-βB turn and part of the βB strand in the second subunit, and vice versa (Leijonmarck and Liljas 1987). Thus, the collective motion of the right handed $\alpha\alpha$-corner that is found in the monomer can be mediated via the dimer interface, resulting in flexibility of the entire dimer structure. This fact may improve the adaptive potentiality to interact with other protein molecules, such as elongation factors. The right handed $\alpha\alpha$-corner is a fairly common structural feature in proteins (Efimov 1984). It appears e.g. in the DNA binding proteins Cro and CAP (Takeda et al. 1983), and its dynamic flexibility may be of importance in binding (Pabo and Sauer 1984).

Adding a restraining energy of roughly 37 kcal/mol, is sufficient to force the CTF dimer into its X-ray conformation. It corresponds in this case to 0.8 kcal/mol per restrained atom. This energy is smaller than the one lost by breaking hydrogen bonds between uncharged side chains, i.e. with a few intermolecular H-bonds the restraining energy can be achieved. In this sense, the dimeric form of CTF could act as an energy transducer when interacting with other proteins.

The 50S ribosomal subunit contains four molecules of L7/L12 (Hardy 1975; Subramanian 1975) but the arrangement of these is not yet established. However, the functional unit is a dimer (Koteliansky et al. 1978) with the *N*-terminal domain being essential for dimer formation (Gudkov and Behlke 1978). Both dimers are associated with their *N*-termini to another ribosomal protein (L10) (Pettersson and Liljas 1979; Gudkov et al. 1982), located at the base of the "L7/L12 stalk". The hinge region (Leijonmarck et al. 1981) suggests the possibility of large movements for the stable *C*-terminal domain (Gudkov et al. 1982), which can explain the different proposed locations of CTF (Möller et al. 1983).

In the CTF monomer the most conserved sequence region is found in the αA-αB motif, which renders it a possible functional site. This conserved region is further extended to a larger area, "footprint" (Leijon-

marck et al. 1984), on the formation of the symmetric dimer observed in the X-ray structure (Leijonmarck and Liljas 1987). The MD calculations indicate that this dimer is not merely an artefact of the crystallisation, but that an even more stable dimer can form if the exact crystallographic symmetry is broken. Furthermore, some L7/L12 mutants, differing at the border of the "footprint", show reduced efficiency in protein synthesis (Liljas et al. 1986). Hence, it seems likely that this dimer exists, at least transiently at some stage, and has possibilities to interact with factors in the translation machinery. Whether the two CTF monomers in this dimer belong to the same *N*-terminal dimer is not known, but both the symmetric parallel model (cf. Fig. 28 of Liljas 1982) and the antiparallel model (Behlke and Gudkov 1980) would allow this type of interaction.

Acknowledgements. Support from the Swedish Natural Science Research Council, including supercomputing facilities, is gratefully acknowledged. We wish to thank Dr. A. Liljas for useful discusssions.

References

Ahlström P, Teleman O, Jönsson B, Forsén S (1987) Molecular dynamics simulation of parvalbumin in aqueous solution. J Am Chem Soc 109:1541–1551

Åqvist J (1986) A simple way to calculate the axis of an α-helix. Comput Chem 10:97–99

Åqvist J, van Gunsteren WF, Leijonmarck M, Tapia O (1985) A molecular dynamics study of the *C*-terminal fragment of the L7/L12 ribosomal protein. Secondary structure motion in a 150 picosecond trajectory. J Mol Biol 183:461–477

Åqvist J, Sandblom P, Jones TA, Newcomer ME, van Gunsteren WF, Tapia O (1986) Molecular dynamics simulations of the holo and apo forms of retinol binding protein. Structural and dynamical changes induced by retinol removal. J Mol Biol 192:593–604

Behlke J, Gudkov AT (1980) Interactions between the ribosomal proteins L7/L12 and L10 as well as L7/L12-L10 and L11 from Escherichia coli. Stud Biophys 81:169–170

Berendsen HJC, Postma JPM, van Gunsteren WF, Hermans J (1981) Interaction models for water in relation to protein hydration. In: Pullman B (ed) Intermolecular forces. Reidel, Dordrecht, Holland, pp 331–342

Berendsen HJC, Postma JPM, Di Nola A, van Gunsteren WF, Haak JR (1984) Molecular dynamics with coupling to an external bath. J Chem Phys 81:3684–3690

Connolly ML (1983) Analytical molecular surface calculation. J Appl Crystallogr 16:548–558

Cowgill CA, Nichols BG, Kenny JW, Butler P, Bradbury EM, Traut RR (1984) Mobile domains in ribosomes revealed by proteon nuclear magnetic resonance. J Biol Chem 259: 15257–15263

Efimov AV (1984) A novel super-secondary structure of proteins and the relation between the structure and the amino acid sequence. FEBS Lett 166:33–38

Fersht AR, Shi J-P, Knill-Jones J, Lowe DM, Wilkinson AJ, Blow DM, Brick P, Carter P, Waye MMY, Winter G (1985) Hydrogen bonding and biological specificity analysed by protein engineering. Nature 314:235–238

Gudkov AT, Behlke J (1978) The *N*-terminal sequence protein of L7/L12 is responsible for its dimerization. Eur J Biochem 90:309–312

Gudkov AT, Gongadze GM (1984) The L7/L12 proteins change conformation upon interaction of EF-G with ribosomes. FEBS Lett 176:32–36

Gudkov AT, Gongadze GM, Bushuev VN, Okon MS (1982) Proton nuclear magnetic resonance study of the ribosomal protein L7/L12 in situ. FEBS Lett 138:229–232

Gunsteren WF van, Berendsen HJC (1977) Algorithms for macromolecular dynamics and constraint dynamics. Mol Phys 34:1311–1327

Hardy SJS (1975) Stoichiometry of the ribosomal proteins of Escherichia coli. Mol Gen Genet 140:253–274

Kabsch W, Sander C (1983) Dictionary of protein secondary structure: Pattern recognition of hydrogen bonded and geometrical features. Biopolymers 22:2577–2637

Koteliansky VE, Domogatsky SP, Gudkov AT (1978) Dimer state of protein L7/L12 and EF-G-dependent reactions on ribosomes. Eur J Biochem 90:319–323

Kuriyan J, Petsko GA, Levy RM, Karplus M (1986) Effect of anisotropy and anharmonicity on protein crystallographic refinement. An evaluation by molecular dynamics. J Mol Biol 190:227–254

Leijonmarck M, Liljas A (1987) Structure of the *C*-terminal domain of the ribosomal protein L7/L12 from Escherichia coli at 1.7 Å. J Mol Biol 195:555–580

Leijonmarck M. Liljas A, Subramanian AR (1984) Computed spatial homology between the L12 protein of chloroplast ribosome and 1.7 Å structure of Escherichia coli L12 domain. Biochem Int 8:69–76

Liljas A (1982) Structural studies of ribosomes. Prog Biophys Mol Biol 40:161–228

Liljas A, Kirsebom L, Leijonmarck M (1986) Structural studies of the factor binding domain. In: Hardesty B, Kramer G (eds) Structure, function and genetics of ribosomes. Springer, Berlin Heidelberg New York, pp 379–390

Möller W, Schrier PI, Maassen JA, Zantema A, Schop E, Reinalda H (1983) Ribosomal proteins L7/L12 of Escherichia coli. Localization and possible molecular mechanism in translation. J Mol Biol 163:553–573

Möller W (1974) The ribosomal components involved in EF-G- and EF-Tu-dependent GTP hydrolysis. In: Nomura M, Tissières A, Lengyel P (eds) Ribosomes. Cold Spring Harbor Laboratory Press, Cold Spring Harbor, New York, pp 711–731

Pabo CO, Sauer RT (1984) Protein-DNA recognition. Annu Rev Biochem 53:293–321

Pettersson I, Kurland CG (1980) Ribosomal protein L7/L12 is required for optimal translation. Proc Natl Acad Sci USA 77:4007–4010

Pettersson I, Liljas A (1979) The stoichiometry and reconstruction of a stable protein complex from Escherichia coli ribosomes. FEBS Lett 98:139–144

Subramanian AR (1975) Copies of proteins L7 and L12 and heterogeneity of the large subunit of Escherichia coli ribosome. J Mol Biol 95:1–8

Tainer JA, Getzoff ED, Beem KM, Richardson JS, Richardson DC (1982) Determination and analysis of the 2 Å structure of copper, zinc superoxide dismutase. J Mol Biol 160:181–217

Takeda Y, Ohlendorf DH, Anderson WF, Matthews BW (1983) DNA-binding proteins. Science 221:1020–1026